Biogeosciences Discuss., https://doi.org/10.5194/bg-2018-468
Manuscript under review for journal Biogeosciences
Discussion started: 6 December 2018

Estimation of emissions from biomass burning in China (2003-2017) based on MODIS fire radiative energy data

Lifei Yin, Pin Du, Mingxu Liu, Tingting Xu, Yu Song

State Key Joint Laboratory of Environmental Simulation and Pollution Control, Department of Environmental Science, Peking University, Beijing, China

Correspondence to: Yu Song (songyu@pku.edu.cn)

Abstract. Biomass burning plays a significant role in air pollution and climate change. In this study, we used the method based on fire radiative energy (FRE) to develop a biomass burning emission inventory for China from 2003 to 2017. Daily fire radiative power (FRP) data in 1 km MODIS Thermal Anomalies/Fire products (MOD14/MYD14) were used to calculate FRE and combusted biomass. Available emission factors were assigned to four land-cover types: forest, cropland, grassland and shrubland. The farming system and crop types in different climate zones were taken into account in this research. Compared with traditional methods, the FRE method was found to provide a more reasonable estimates of emissions from small fires. The estimated average annual emission ranges, with a 90% confidence interval, were 94.2 (78.7-117.6) Tg CO_2 yr^{-1}, 4.9 (2.5-8.3) Tg CO yr^{-1}, 0.19 (0.05-0.51) Tg CH_4 yr^{-1}, 0.52 (0.18-0.81) Tg NMHC yr^{-1}, 0.18 (0.04-0.39) Tg NO_x yr^{-1}, 0.07 (0.02-0.17) Tg NH_3 yr^{-1}, 0.03 (0.01-0.06) Tg SO_2 yr^{-1}, 0.04 (0.01-0.08) Tg BC yr^{-1}, 0.3 (0.08-0.53) Tg OC yr^{-1}, 0.49 (0.20-0.88) Tg $PM_{2.5}$ yr^{-1}, 0.56 (0.16-1.11) Tg PM_{10} yr^{-1}. Forest fire was identified as the major source of the biomass burning emissions, and crop residue burning was the second highest contributor. In the 15-year study period, emissions from forest fires showed a significant downward trend. Crop residue emissions continued to rise until 2014, and then began to decline. Emissions from grassland and shrubland were little changed. Forest, grassland, and shrubland fires are mostly located in regions with high vegetation coverage, where the occurrence of fires is concentrated in arid seasons (spring and autumn). Plain areas with high crop yields, such as the North China Plain, experienced high agricultural fire emissions in harvest seasons. The resolution (daily, 1 km) of our inventory is much higher than previous inventories, such as GFED4s and GFASv1.0. It could be used in global and regional air quality modeling.

Biogeosciences Discuss., https://doi.org/10.5194/bg-2018-468
Manuscript under review for journal Biogeosciences
Discussion started: 6 December 2018

1. Introduction

Biomass burning is an important source of gaseous and particulate matter emissions to the troposphere (Crutzen et al., 1979; Seiler and Crutzen, 1980). Globally, biomass burning contributes around 20 %–30 % of CO_2 emissions and chemically active gases such as hydrocarbons, CO and NO_x (Andreae, 1991), approximately 42 % of black carbon (BC), and 74 % of primary organic carbon (OC) (Bond et al., 2004). These compounds have significant impacts on air quality, atmospheric chemistry, climate change, and human health (Andreae et al., 1994; Reid et al., 2005).

China is a large agricultural country, and vast amounts of crop residues are burned in field each year, leading to substantial pollutant emissions. Emission from biomass burning in other ecosystems, such as forest fires, are also of great concern (Chen et al., 2017). Three methods are frequently used to estimate open fire emissions. First, statistical data distributed by Chinese national government are used to develop nationwide emission inventories (Cao et al., 2005; Lu et al., 2011; Yan et al., 2006). This method requires multiple parameters that depend on local conditions (Huang et al., 2012; Yan et al., 2006), leading to high uncertainty. Moreover, this method produces emission estimates at a coarse resolution that does not permit detailed analysis of spatiotemporal patterns. Second, an approach based on fire count data provided by satellite observation of active fire is also widely used. Mehmood et al. (2018) analyzed the spatiotemporal distribution of emissions from biomass burning in China using data derived from the Fire INventory from NCAR version 1.0 (FINNv1), which was developed from the fire count method (Wiedinmyer et al., 2011). In this approach, a maximum burned area of 1 km^2 is assumed for each fire detected. Because the actual burned area can vary greatly, this method is likely to overestimate burned area for small fires and underestimate that for fires spreading to larger areas (Wiedinmyer et al., 2006; Song et al., 2009). The third method is based on a satellite dataset of burned areas, with emissions typically calculated as the product of burned area, fuel load, combustion factor, and emission factor (Seiler and Crutzen, 1980; Song et al., 2009; Chang and Song, 2010). Many factors in the equation, such as fuel load and combustion factor, are highly variable with local characteristics (e.g., climatic conditions and fuel moisture) and difficult to ascertain. Besides, Song et al. (2009) found that this method significantly underestimated farmland fire emissions because crop residue fires may be too small for efficient satellite detection. All of these methods depend strongly on burned area and require multiple parameters. Although many studies have combined these methods to improve estimates

(Zhou et al., 2017; Wu et al., 2018; Qiu et al., 2016; Huang et al., 2012), the accumulation of uncertainties from these factors can significantly influence results.

Recently, an approach based on fire radiative energy (FRE) has increasingly been used. FRE is the amount of energy radiated during the combustion process (Kaufman et al., 1996). A strong linear relationship has been demonstrated between FRE and fuel mass consumed; the coefficient of this relationship is insensitive to vegetation type (Freeborn et al., 2008; Wooster, 2002). Therefore, the amount of pollutant produced by combustion can be calculated as the product of FRE-derived fuel mass and a corresponding emission factor. Fire radiative power (FRP), or instantaneous FRE, typically recorded in active fire datasets from satellite observations, is used to determine FRE by integration over the lifespan of a fire event (Vermote et al., 2009). A key feature of this method is that it calculates fuel mass as the product of FRE and a conversion ratio, reducing uncertainty due to multiple parameters. Liu et al. (2015) applied this approach to investigate the characteristic and pollutants emissions of winter wheat burning in North China Plain during the harvest season (June in that study). A comparison of their results with those of Huang et al. (2012) suggested that the approach produced a reasonable estimation. According to the accumulated temperature, China is divided into five temperature zones (tropical zone, subtropical zone, and warm-/middle-/cold–temperate zone) (Shi, 2015). The growth period varies among temperature zones and the farming system and crop types are also significantly different. For example, in tropical regions, the staple crops are rice, sugarcane and natural rubber, and rice grown there could be harvested for three times per year. While in middle-temperate zone, the main crops are spring wheat, maize and soybean, which ripen only once a year. This method parameterizes the FRP diurnal cycle for crop zones and harvest seasons, which could show specific combustion characteristic for different straw types. Few studies have used this approach to estimate emissions from agricultural burning on a national scale. Thus, a comprehensive biomass burning emission inventory for the whole China is needed.

In this study, we used daily FRP data from 1 km the MODIS active fire products to calculate emissions of 11 pollutants from biomass burning in China (excluding fires occurring on the small islands in the South China Sea) from 2003 to 2017. The GlobCover 2009 dataset was used to define biomass types (forest, grassland, cropland, and shrubland). A comprehensive daily gridded 1 km inventory of biomass burning emission was established; this inventory could meet the requirements of global and regional air quality simulations.

Biogeosciences Discuss., https://doi.org/10.5194/bg-2018-468
Manuscript under review for journal Biogeosciences
Discussion started: 6 December 2018

2. Methods and data

2.1 Methods

Pollutant emissions were calculated as the product of dry mass burned (kg) and a corresponding emission factor (g kg^{-1}). In this study, emission factors for each land-cover type were derived from published studies (Table S1).

Due to the excellent linear relationship between FRE and combusted dry matter, biomass fuel mass could be estimated by multiplying FRE by a specific conversion ratio, which was not significantly influenced by vegetation types (Wooster et al., 2005):

$$M = FRE \times CR \quad (1)$$

Where M is the dry biomass consumed of one grid cell, FRE is the total radiative energy during the fire lifespan for one grid cell, and CR is the conversion ratio (kg MJ^{-1}) used to convert FRE to combusted biomass.

Wooster et al. (2005) reported a conversion ratio of 0.368±0.015 kg MJ^{-1}, and that evaluated by Freeborn et al. (2008) was 0.453±0.068 kg MJ^{-1}. In this study, we used the average value (0.411 kg MJ^{-1}).

FRE was estimated by integrating FRP (i.e. instantaneous FRE) over the duration of the fire process. In this study, FRP data from MODIS active fire products were used. The MODIS sensors, onboard the polar-orbiting satellites Terra and Aqua, acquire four discrete FRP data at 1030 and 2230 (Terra) and 0130 and 1330 (Aqua), equatorial local time.

Vermote et al. (2009) proposed a modified Gaussian function to parameterize the FRP diurnal cycle based on the long-term ratio between Terra and Aqua FRP (T/A ratio). This parameterization describes the discrete observations as a continuous function and subsequently simplifies integral process to estimate total fire energy released. The modified Gaussian function is:

$$FRE = \int FRP = \int_0^{24} FRP_{peak}\,(b + e^{-\frac{(t-h)^2}{2\sigma^2}})dt \quad (2)$$

Where FRP_{peak} represents the peak of the diurnal cycle, b represents the background FRP, σ represents the standard deviation of the curve, and h represents the hour of peak FRP.

In this study, we used monthly T/A ratio to determine the parameters in the function. The empirical relationship between these variables and T/A ratio could be found in Vermote et al. (2009). It is important to note that the origin formula of calculating h

could not provide reasonable estimations. Although it has been pointed that the variable *h* has little effect on the final calculation of FRE, we decided to add a parameter ε that was introduced by Liu et al. (2015) in order to modify FRP peak hour. The modified equation was:

$$h = -1.23x + 14.57 + \varepsilon \quad (3)$$

Where *x* represented the monthly T/A ratio.

2.2 Data

The MODIS Thermal Anomalies/Fire 5-Min L2 Swath Products (MOD14/MYD14) were derived from MODIS 4- and 11-micrometer radiances. The products provide the location, FRP and other information of fire events with moderate spatial resolution (1 km^2) and high temporal resolution (daily). MOD14 data were obtained from Terra, which passes at 10:30 and 22:30 local time (LT), and MYD14 data were provided by Aqua, which acquires observations at 01:30 and 13:30 LT. We used data for a 15-year period (2003–2017) to calculate FRE and estimate emissions.

The GlobCover 2009 land cover product, which is processed by the European Space Agency (ESA) and the Université Catholique de Louvain (Bicheron et al., 2008), was applied to differentiate land-cover types. GlobCover 2009 is the most detailed map of Earth land surface with a spatial resolution of 300 m (Arino et al., 2008). In this study, we grouped the 22 land-cover types provided by the product into five broad types: forest, shrubland, grassland, cropland, and others (Figure S1). We combined the land-cover map of China and the latitude and longitude data of fire count provided in MOD14/MYD14 to determine the fire types. For instance, if a fire count is detected in cropland area, then it will be considered as a crop residue burning event.

To compare the results, we also computed the pollutant emissions using data derived from MODIS burned area products (MCD64A1, http://modis-fire.umd.edu/), the fourth version of the Global Fire Emission Database (with small fires) (GFED4s, Van Der Werf et al. (2017), Giglio et al. (2013), Randerson et al. (2012)), Global Fire Assimilation System (GFASv1.0, Kaiser et al. (2012)), and FINNv1.5 (http://bai.acom.ucar.edu/Data/fire/). We derived data for 2003–2017 from MCD64A1, which is a monthly, global gridded 500 m product containing per-pixel burned area information. We applied the monthly emission data

at a spatial resolution of 0.25° in GFED4s; the latest GFED4s data are for 2016. GFASv1.0 calculates daily biomass burning emissions by assimilating FRP data from MODIS sensors on a global 0.5°×0.5° grid (Kaiser et al., 2012); we used GFASv1.0 data to estimate emission from 2003 to 2013. FINNv1.5 provides daily high-resolution (1 km) emissions of global biomass burning; data from 2003 to 2016 were used for comparison in this study.

3. Results and discussion

A total of 462,525 biomass fire pixels were detected by Terra, and 492,822 by Aqua from 2003 to 2017. When a fire pixel was probed by both satellites within the same day, we removed the Terra pixel to avoid repeated computations. Thus, a total of 942,933 fire pixels were applied to estimate emissions. The inter-annual variation in emissions was shown in Table 1. For the 15-year study period, average emissions of CO_2, CO, CH_4, NMHC, NO_x, NH_3, SO_2, BC, OC, $PM_{2.5}$, and PM_{10} were estimated to be 94.2, 4.9, 0.19, 0.52, 0.18, 0.07, 0.03, 0.04, 0.30, 0.49 and 0.56 Tg yr^{-1}, respectively. Taking CO2 emission as an example, the maximum emission occurred in 2003 (129.1 Tg), followed by 2014 (121.4 Tg) and 2009 (108.5 Tg), and the minimum emission occurred in 2017 (61.0 Tg). These results will be discussed in detail in Section 3.2.

3.1 Spatial distribution of emissions

Average annual emissions of 11 pollutants at the provincial level were listed in Table 2, and source-specific emissions of CO_2 for each province were presented in Fig.1. Using CO_2 as a representative example, southwestern and northeastern China were the most significant emitters, contributing 52 % to the total emissions, most of which were derived from forest and grassland fires. The result was in connection with rural population intensity and land use patterns (Qiu et al., 2016). For example, the highest emission amount was found in Heilongjiang due to its abundant forest and grassland resources in Daxing'anling and Xiaoxing'anling. The southwestern region, on the Yunnan-Guizhou Plateau, was also densely forested. Careless fire starting and unfavorable weather in dry seasons could easily lead to severe forest fires (Lintao, 1999). Approximately 80 % of fire emissions in central and northern regions were derived from agricultural fires. Benefiting from fertile land and favorable climate, these two regions contain several major agricultural provinces, such as Shandong, Henan, Hunan, and Anhui Provinces, where large amounts of crop residues were burned during harvest seasons. Southeastern provinces in the Middle-Lower

Yangtze River Plain and the southeastern hills had abundant cultivated land and forest resources, resulting in relatively high CO_2 emissions from cropland and forest fires. Due to water shortages and barren land in northwestern China, arbor and bush species barely survived there, leading to negligible emissions from biomass burning. For instance, CO_2 emissions from Ningxia and Qinghai were 0.20 Tg yr^{-1} and 0.94 Tg yr^{-1}, respectively. Vegetation in these areas consisted of grass and a few drought-resistant crops; hence, an extremely high proportion (97 %) of CO_2 emissions in the northwest arose from grassland and cropland fires.

Nationwide allocation of CO_2 emissions from four sources was shown in Fig. 2 (excluding biomass fire emissions from the small islands in the South China Sea). Forest and grassland fire emissions were clearly mainly distributed in northeastern and southern China. These regions were dominated by landforms that are favorable for growing trees and grass, including high plateaus (e.g., Yunnan-Guizhou Plateau, Inner Mongolian Plateau), mountain ranges (e.g., Daxing' anling, Xiaoxing'anling) and hills (e.g., the southeast hills). High-intensity cropland fire emissions occurred in the three great plains of China: the Northeast China Plain, the North China Plain, and the Middle–Lower Yangtze Plain. Due to high crop production in these areas, great amounts of agricultural residues were burned in fields during the short period following the harvest season. Due to snowmelt in the Tianshan Mountains, there are many oases at the foot of the mountain range in Xinjiang Province. These oases are suitable for growing crops such as wheat and maize (Zhou et al., 2017). Therefore, crop fire emissions in Xinjiang were higher than those in other northwestern provinces in China. Finally, emissions from shrubland fire were concentrated in the south due to bush growth.

3.2 Temporal pattern of emissions

The annul variations of total and source–specific CO_2 emissions were presented in Fig.3. Peak emissions occurred in 2003, 2009 and 2014, with major contributors of forest in 2003 (58 %) and 2009 (44 %), and cropland fire in 2014 (41 %). According to the China Forestry Statistical Yearbook, there are seven extraordinarily serious fire accidents in 2003, causing the largest forest burned area in the study period. There are 35 serious fire accidents happened in 2009, 171 % higher than the 15-year average number of that kind of events (12.9). Forest fires are well controlled after 2003, while the pollutants from residue burning continue to rise, and reach peak in 2014, leading to 49.8 Tg CO_2 emission in a year. Discharge from forest fire

decreased from 73.7 Tg in 2003 to 19.9 Tg in 2017. As over 95 % of forest fires in China are caused by careless or deliberate human activities, the implement of strict forest conservation policies and the development of fire control technology contribute significantly to the emission decline (Huang et al., 2011). Grassland and shrubland fire emissions remained relatively stable during the study period. Emissions from forest, grassland and shrubland exhibited a small peak in 2014. According to the statics, the total burned areas in 2014 of both forest and grassland are higher than previous years. The rise in burned area and emission could be attributed to an unusual warm condition occurred in 2014, which could facilitate the occurrence and spread of fires (Bond et al., 2015). Emissions from cropland continued to rise until 2014, and then began to decline. This trend was similar to that reported by Zhuang et al. (2018). The rising trend could be caused by economic development and urbanization, which lead to a decline in biofuel use as an energy source. As a result, crop residues were increasingly burned in the field (Yan et al., 2006). Due to the serious haze experienced across China in the winter of 2013 and demonstrations by researchers of the effects of biomass burning, the Chinese government implemented a series of policies and measures to improve air quality. Agricultural residue burning has been under restriction since that period, and cropland emissions have decreased rapidly since 2014.

Monthly mean CO_2 emissions during 2003-2017 from each source were presented in Fig.4. Spring months (March, April and May) contributed most (41 %) of the total CO_2 emission yearly due to the arid climate, low vegetation moisture, high wind speed, and other unfavorable conditions that facilitate the start and spread of fires (Song et al., 2009). Li et al. (2015) showed that a large portion of forest fires in spring were caused by “paper money” burning in Tomb-sweeping Day (April 5). The emission of 11.13 Tg CO_2 in June (78 % of total emissions) was due to agricultural fires. The lowest emissions occurred during midsummer and early autumn (July, August, and September), producing 2.8, 2.3, and 2.0 Tg CO_2, respectively. These low values may be resulted by the plentiful precipitation, which reduced fuel flammability. An emission peak was detected in late autumn, which could be attributable to crop harvest and weather conditions that easy to induce combustion in forest and grassland, just like that in spring. Winter emissions, which chiefly arose from forest and grassland fires, were lower than those in spring and late autumn, but higher than those in summer. Fires in winter were concentrated in southern China due to low precipitation and mild temperatures. In contrast, boreal forests rarely burned due to low temperatures and moist snow cover.

This result was consistent with the findings of Chen et al. (2017) that extensive forest fires occurred in southern and northeastern China during spring and southern China during winter.

As shown in Fig.4, except for agricultural fire, other fire types including forest, grassland, and shrubland fires exhibited similar temporal allocation, i.e., higher emissions in spring, late autumn and winter and lower emissions in summer. This pattern was strongly affected by unfavorable weather conditions. However, emissions from crop burning exhibited clear seasonal variation that was closely related to agriculture activities. High emissions occurred in early summer, and small peaks were detected in spring and autumn. Different staple crops and sowing/harvest times in different areas could lead to multiple emission peaks (Jin et al., 2018; Zhou et al., 2017). From March to May, as large amounts of crop residues were burned to clear the cultivated land for later sowing, fires were scattered throughout the country. During summer, crop burning was concentrated in the North China Plain due to winter wheat and maize straw combustion. During autumn (especially October), second-round rice straw burning in south China was a primary contributor, and small areas of maize residue burning were detected in north China (Chen et al., 2017). During winter, crop burning occurred most frequently in southern China, perhaps due to burning activity prior to soybean sowing (Zhou et al., 2017).

3.3 Comparison with other studies

The average annual emission estimates produced in this study were compared to those based on data from the MCD64A1, GFED4s, GFASv1.0, and FINNv1.5 (Table 3). Generally, our results were closed to those from GFED4s and GFASv1, indicating that this method produced a reasonable estimation. However, estimates based on the burned area product were lower than our results. The high omission rate of small fires could be a dominant factor contributing to this discrepancy (Tansey et al., 2008). Emission estimates by FINNv1.5 were higher than those of this study, with a difference ranging from 24 % to 172 %. This result was consistent to a study by Wiedinmyer et al. (2011), which suggested that FINNv1 tends to predict higher emissions for Southeast Asia.

A comparison of average emissions from four fire types was presented in Table 4 (shrubland and grassland fires are lumped into one category in GFED4s). Due to shielding by the dense canopy (Moreira de Araújo et al., 2012; Roy and Boschetti, 2009) and high small-fire omission rates, emissions derived from burned area methods were underestimated by 72 %–92 %,

especially for shrubland fire (–92 %) and cropland fire (–92 %) emissions. Our results were slightly higher than those of GFED4s for forest and grassland fire but lower than those of GFED4s for cropland fire emissions. Datasets in GFED4s are based on burned area boosted by small fire burned area, which could provide a relatively high emission estimation of agricultural fires. FINNv1.5 emission estimates were higher for forest and shrubland, perhaps due to the burned area assumption (Song et al., 2009) and land cover identification (wood grassland was lumped in shrubland category). Estimates of grassland and cropland fire emissions in FINNv1.5 were similar to our results, with differences of –20 % and 21 %, respectively. In conclusion, our estimates were higher than those based on burned area products due to lower uncertainties from parameters and more reasonable estimates of small fire emissions. These results were similar to those from FINNv1.5 in terms of emissions from grassland and cropland fires and very close to those from GFED4s and GFASv1 for all fire types. Therefore, this method developed an inventory with higher spatiotemporal resolution and improved estimation of biomass burning emissions, especially for small fires in shrubland and cropland.

4 Uncertainty

Several sources of error impact the accuracy of our estimate. The first error source is related to the radiative energy diurnal cycle parameterization that impacts the calculation of FRE. In addition, the error in the fire detection and empirical formula for computing FRP have a considerable impact on the accuracy of FRE. The use of the conversion ratio in order to convert FRE to combusted biomass is one of error sources as well. According to the error budget presented by Vermote et al. (2009), we assumed that the relative error of FRE and the conversion ratio was 31 % and 10 %, respectively. Since emission factors vary in time and space, they could bring about large uncertainties in the emission estimates. The uncertainty of the EF is species dependent and we applied the uncertainty suggested in Huang et al. (2012). We ran 20,000 Monte Carlo simulations to estimate the range of average annual fire emissions in 2003-2017 with a 90 % confidence interval. The estimated emissions of CO_2, CO, CH_4, NMHC, NO_x, NH_3, SO_2, BC, OC, $PM_{2.5}$ and PM_{10} were 94.2 (78.7-117.6), 4.9 (2.5-8.3), 0.19 (0.05-0.51), 0.52 (0.18-0.81), 0.18 (0.04-0.39), 0.07 (0.02-0.17), 0.03 (0.01-0.06), 0.04 (0.01-0.08), 0.3 (0.08-0.53), 0.49 (0.20-0.88), and 0.56 (0.16-1.11) Tg yr^{-1}, respectively.

Biogeosciences Discuss., https://doi.org/10.5194/bg-2018-468
Manuscript under review for journal Biogeosciences
Discussion started: 6 December 2018

5 Conclusion

In this study, we developed a high-spatiotemporal-resolution (daily data in a 1 km×1 km grid) inventory of emissions from biomass burning in China based on MODIS FRP data. The annual average emissions of were 94.2 (78.7-117.6), 4.9 (2.5-8.3), 0.19 (0.05-0.51), 0.18 (0.04-0.39), 0.04 (0.01-0.08), 0.3 (0.08-0.53), and 0.49 (0.20-0.88) Tg yr^{-1} for CO_2, CO, CH_4, NO_x, BC, OC, and $PM_{2.5}$, respectively. Emissions in southwestern and northeastern China contributed most to the total, at a proportion of 52 %. Spatially, forest and grassland fires were concentrated in northeastern, southeastern, and southwestern regions. Cropland fires were common in the Northeast China Plain, the North China Plain, and the Middle–Lower Yangtze Plain, and shrubland fire occurred frequently in the south. Temporally, total emissions were relatively high in 2003 and 2014, and the lowest emissions occurred in 2017. Most natural fires from forest, grassland and shrubland occurred during the dry seasons (spring and autumn), whereas agricultural fires were concentrated in the harvest months (June and October). Compared with estimations by other methods, our results are much higher than those obtained by the burned area method due to more accurate calculation of small fire emissions, and lower than those by FINNv1.5 for forest and shrubland fire emissions. Our estimates were very close to those from GFED4s and GFASv1.0, as well as grassland and cropland fire emissions from FINNv1.5, indicating that our results were reasonable and can be used for further research. Uncertainties in our estimates may have been caused by many factors such as the characterization of the fire energy radiative diurnal cycle; thus, future studies should seek to improve the accuracy of the method.

Data availability. MODIS data can be freely accessed at https://search.earthdata.nasa.gov/search. GlobCover data are downloaded from European Space Agency data user element website (http://due.esrin.esa.int/page_globcover.php). GFASv1.0 data are available on http://apps.ecmwf.int/datasets/data/cams-gfas/. GFED4s data can be downloaded from https://daac.ornl.gov/VEGETATION/guides/fire_emissions_v4.html. FINNv1.5 data can be found at http://bai.acom.ucar.edu/Data/fire/.

Author contributions. This work was designed by YS and performed by LY, PD, ML, and TX. LY and YS led the writing of the papers and prepared the figures with contributions from all co-authors.

Competing interests. The authors declare that they have no conflict of interest.

Acknowledgements. The MODIS Thermal Anomalies/Fire products (MOD14/MYD14) and burned area product (MCD64A1) were provided by Land Process Distributed Active Archive Center (LPDAAC), USA. The GlobCover 2009 land cover product was provided by the European Space Agency (ESA). This study was funded by National Key R&D Program of China (2016YFC0201505) and National Natural Science Foundation of China (NSFC) (91644212 and 41675142).

References

Andreae, M., Fishman, J., Garstang, M., Goldammer, J., Justice, C., Levine, J., Scholes, R., Stocks, B., Thompson, A., and Van Wilgen, B.: Biomass Burning in the Global Environment: First Results from the IGAC/BIBEX Field Campaign STARE/TRACE-A/SAFARI-92, in: Global atmospheric-biospheric chemistry, Springer, 83-101, 1994.

Andreae, M. O.: Biomass burning: its history, use, and distribution and its impact, in, Global Biomass Burning: Atmospheric, Climatic, and Biospheric Implications [JS Levine (Ed.)]. Cambridge, MA, MIT Press, 1991.

Arino, O., Bicheron, P., Achard, F., Latham, J., Witt, R., and Weber, J. L.: GLOBCOVER The most detailed portrait of Earth, Esa Bulletin-European Space Agency, 24-31, <Go to ISI>://WOS:000261325400042008.

Bicheron, P., Defourny, P., Brockmann, C., Schouten, L., and Vancutsem, C.: GLOBCOVER: products description and validation report, Foro Mundial De La Salud, 17, 285-287, 2008.

Bond, N. A., Cronin, M. F., Freeland, H., and Mantua, N.: Causes and impacts of the 2014 warm anomaly in the NE Pacific, Geophysical Research Letters, 42, 3414-3420, 2015.

Bond, T. C., Streets, D. G., Yarber, K. F., Nelson, S. M., Woo, J.-H., and Klimont, Z.: A technology-based global inventory of black and organic carbon emissions from combustion, Journal of Geophysical Research: Atmospheres, 109, doi:10.1029/2003JD003697, 2004.

Cao, G., Zhang, X., Wang, D., and Zheng, F.: Inventory of atmospheric pollutants discharged from biomass burning in China continent, China Environmental Science, 25, 389-393, 2005.

Chang, D., and Song, Y.: Estimates of biomass burning emissions in tropical Asia based on satellite-derived data, Atmospheric Chemistry and Physics, 10, 2335-2351, 2010.

Chen, J., Li, C., Ristovski, Z., Milic, A., Gu, Y., Islam, M. S., Wang, S., Hao, J., Zhang, H., He, C., Guo, H., Fu, H., Miljevic, B., Morawska, L., Thai, P., Lam, Y. F., Pereira, G., Ding, A., Huang, X., and Dumka, U. C.: A review of biomass burning: Emissions and impacts on air quality, health and climate in China, Science of The Total Environment, 579, 1000-1034, doi:https://doi.org/10.1016/j.scitotenv.2016.11.025, 2017.

Crutzen, P. J., Heidt, L. E., Krasnec, J. P., Pollock, W. H., and Seiler, W.: Biomass burning as a source of atmospheric gases CO, H2, N2O, NO, CH3Cl and COS, Nature, 282, 253, 1979.

Freeborn, P. H., Wooster, M. J., Hao, W. M., Ryan, C. A., Nordgren, B. L., Baker, S. P., and Ichoku, C.: Relationships between energy release, fuel mass loss, and trace gas and aerosol emissions during laboratory biomass fires, Journal of Geophysical Research, 113, doi:10.1029/2007jd008679, 2008.

Giglio, L., Randerson, J. T., and van der Werf, G. R.: Analysis of daily, monthly, and annual burned area using the fourth-generation global fire emissions database (GFED4), Journal of Geophysical Research: Biogeosciences, 118, 317-328, doi:10.1002/jgrg.20042, 2013.

Huang, X., Li, M., Friedli, H. R., Song, Y., Chang, D., and Zhu, L.: Mercury emissions from biomass burning in China, Environmental science & technology, 45, 9442-9448, 2011.

Huang, X., Li, M., Li, J., and Song, Y.: A high-resolution emission inventory of crop burning in fields in China based on MODIS Thermal Anomalies/Fire products, Atmospheric Environment, 50, 9-15, doi:10.1016/j.atmosenv.2012.01.017, 2012.

Jin, Q., Ma, X., Wang, G., Yang, X., and Guo, F.: Dynamics of major air pollutants from crop residue burning in mainland China, 2000–2014, Journal of Environmental Sciences, 70, 190-205, 2018.

Kaiser, J., Heil, A., Andreae, M., Benedetti, A., Chubarova, N., Jones, L., Morcrette, J., Razinger, M., Schultz, M., and Suttie, M.: Biomass burning emissions estimated with a global fire assimilation system based on observed fire radiative power, 2012.

Kaufman, Y. J., Remer, L., Ottmar, R., Ward, D., Li, R. R., Kleidman, R., Fraser, R. S., Flynn, L., McDougal, D., and Shelton, G.: Relationship between remotely sensed fire intensity and rate of emission of smoke: SCAR-C experiment, Global biomass burning, 685-696, 1996.

Li, J., Song, Y., Huang, X., and Li, M.: Comparison of forest burned areas in mainland China derived from MCD45A1 and data recorded in yearbooks from 2001 to 2011, International Journal of Wildland Fire, 24, 103-113, 2015.

Lintao, S. L. T. X. M.: THE STATUS AND COUNTERMEASURE RESEARCH OF FOREST FIRE DISASTERS IN CHINA [J], JOURNAL OF CATASTROPHOLOGY, 3, 020, 1999.

Liu, M., Song, Y., Yao, H., Kang, Y., Li, M., Huang, X., and Hu, M.: Estimating emissions from agricultural fires in the North China Plain based on MODIS fire radiative power, Atmospheric Environment, 112, 326-334, doi:10.1016/j.atmosenv.2015.04.058, 2015.

Lu, B., Kong, S., Han, B., Wang, X., and Bai, Z.: Inventory of atmospheric pollutants discharged from biomass burning in China continent in 2007, China Environmental Science, 31, 186-194, 2011.

Mehmood, K., Chang, S., Yu, S., Wang, L., Li, P., Li, Z., Liu, W., Rosenfeld, D., and Seinfeld, J. H.: Spatial and temporal distributions of air pollutant emissions from open crop straw and biomass burnings in China from 2002 to 2016, Environmental Chemistry Letters, 16, 301-309, 2018.

Moreira de Araújo, F., Ferreira, L. G., and Arantes, A. E.: Distribution Patterns of Burned Areas in the Brazilian Biomes: An Analysis Based on Satellite Data for the 2002–2010 Period, Remote Sensing, 4, 1929-1946, doi:10.3390/rs4071929, 2012.

Qiu, X., Duan, L., Chai, F., Wang, S., Yu, Q., and Wang, S.: Deriving High-Resolution Emission Inventory of Open Biomass Burning in China based on Satellite Observations, Environ Sci Technol, 50, 11779-11786, doi:10.1021/acs.est.6b02705, 2016.

Randerson, J. T., Chen, Y., van der Werf, G. R., Rogers, B. M., and Morton, D. C.: Global burned area and biomass burning emissions from small fires, Journal of Geophysical Research: Biogeosciences, 117, n/a-n/a, doi:10.1029/2012jg002128, 2012.

Reid, J., Koppmann, R., Eck, T., and Eleuterio, D.: A review of biomass burning emissions part II: intensive physical properties of biomass burning particles, Atmospheric Chemistry and Physics, 5, 799-825, 2005.

Roy, D. P., and Boschetti, L.: Southern Africa Validation of the MODIS, L3JRC, and GlobCarbon Burned-Area Products, IEEE Transactions on Geoscience and Remote Sensing, 47, 1032-1044, doi:10.1109/tgrs.2008.2009000, 2009.

Seiler, W., and Crutzen, P. J.: Estimates of gross and net fluxes of carbon between the biosphere and the atmosphere from biomass burning, Climatic Change, 2, 207-247, doi:10.1007/bf00137988, 1980.

Song, Y., Liu, B., Miao, W., Chang, D., and Zhang, Y.: Spatiotemporal variation in nonagricultural open fire emissions in China from 2000 to 2007, Global biogeochemical cycles, 23, 2009.

Tansey, K., Grégoire, J. M., Defourny, P., Leigh, R., Pekel, J. F., Van Bogaert, E., and Bartholomé, E.: A new, global, multi-annual (2000–2007) burnt area product at 1 km resolution, Geophysical Research Letters, 35, 2008.

Van Der Werf, G. R., Randerson, J. T., Giglio, L., Van Leeuwen, T. T., Chen, Y., Rogers, B. M., Mu, M., Van Marle, M. J., Morton, D. C., and Collatz, G. J.: Global fire emissions estimates during 1997-2016, 2017.

Vermote, E., Ellicott, E., Dubovik, O., Lapyonok, T., Chin, M., Giglio, L., and Roberts, G. J.: An approach to estimate global biomass burning emissions of organic and black carbon from MODIS fire radiative power, Journal of Geophysical Research, 114, doi:10.1029/2008jd011188, 2009.

Wiedinmyer, C., Quayle, B., Geron, C., Belote, A., McKenzie, D., Zhang, X., O'Neill, S., and Wynne, K. K.: Estimating emissions from fires in North America for air quality modeling, Atmospheric Environment, 40, 3419-3432, doi:10.1016/j.atmosenv.2006.02.010, 2006.

Wiedinmyer, C., Akagi, S., Yokelson, R. J., Emmons, L., Al-Saadi, J., Orlando, J., and Soja, A.: The Fire INventory from NCAR (FINN): A high resolution global model to estimate the emissions from open burning, Geoscientific Model Development, 4, 625, 2011.

Wooster, M. J.: Small-scale experimental testing of fire radiative energy for quantifying mass combusted in natural vegetation fires, Geophysical Research Letters, 29, 23-21-23-24, 2002.

Wooster, M. J., Roberts, G., Perry, G. L. W., and Kaufman, Y. J.: Retrieval of biomass combustion rates and totals from fire radiative power observations: FRP derivation and calibration relationships between biomass consumption and fire radiative energy release, Journal of Geophysical Research, 110, doi:10.1029/2005jd006318, 2005.

Wu, J., Kong, S., Wu, F., Cheng, Y., Zheng, S., Yan, Q., Zheng, H., Yang, G., Zheng, M., and Liu, D.: Estimating the open biomass burning emissions in central and eastern China from 2003 to 2015 based on satellite observation, Atmospheric Chemistry & Physics, 18, 2018.

Yan, X., Ohara, T., and Akimoto, H.: Bottom-up estimate of biomass burning in mainland China, Atmospheric Environment, 40, 5262-5273, doi:10.1016/j.atmosenv.2006.04.040, 2006.

Zhou, Y., Xing, X., Lang, J., Chen, D., Cheng, S., Lin, W., Xiao, W., and Liu, C.: A comprehensive biomass burning emission inventory with high spatial and temporal resolution in China, Atmospheric Chemistry and Physics, 17, 2839, 2017.

Zhuang, Y., Li, R., Yang, H., Chen, D., Chen, Z., Gao, B., and He, B.: Understanding Temporal and Spatial Distribution of Crop Residue Burning in China from 2003 to 2017 Using MODIS Data, Remote Sensing, 10, 390, 2018.

Biogeosciences Discuss., https://doi.org/10.5194/bg-2018-468
Manuscript under review for journal Biogeosciences
Discussion started: 6 December 2018

Table 1. Biomass burning emissions inventory (Tg) of China from 2003 to 2017.

Year	CO_2	CO	CH_4	NMHC	NO_x	NH_3	SO_2	BC	OC	$PM_{2.5}$	PM_{10}
2003	129.1	6.6	0.26	0.69	0.25	0.08	0.04	0.05	0.47	0.73	0.81
2004	107.9	5.5	0.22	0.59	0.20	0.07	0.03	0.04	0.38	0.60	0.67
2005	76.1	4.0	0.16	0.42	0.15	0.05	0.02	0.03	0.25	0.39	0.45
2006	94.1	4.9	0.19	0.54	0.18	0.06	0.03	0.04	0.32	0.51	0.58
2007	89.1	4.7	0.19	0.52	0.17	0.06	0.03	0.04	0.28	0.46	0.53
2008	106.0	5.5	0.22	0.60	0.20	0.07	0.03	0.04	0.36	0.57	0.65
2009	108.5	5.6	0.22	0.61	0.21	0.07	0.03	0.04	0.36	0.58	0.66
2010	93.2	4.8	0.19	0.52	0.18	0.07	0.03	0.04	0.30	0.48	0.54
2011	80.8	4.2	0.17	0.46	0.16	0.06	0.02	0.03	0.25	0.41	0.47
2012	87.1	4.6	0.18	0.51	0.17	0.07	0.03	0.04	0.25	0.42	0.48
2013	94.3	4.9	0.19	0.54	0.19	0.07	0.03	0.04	0.28	0.47	0.54
2014	121.4	6.3	0.25	0.67	0.24	0.09	0.04	0.05	0.37	0.59	0.69
2015	99.2	5.2	0.20	0.54	0.20	0.07	0.03	0.04	0.29	0.47	0.55
2016	64.8	3.4	0.13	0.35	0.13	0.05	0.02	0.03	0.19	0.31	0.36
2017	61.0	3.1	0.12	0.30	0.12	0.04	0.02	0.02	0.21	0.32	0.36
Average	94.2	4.9	0.19	0.52	0.18	0.07	0.03	0.04	0.30	0.49	0.56

Biogeosciences Discuss., https://doi.org/10.5194/bg-2018-468
Manuscript under review for journal Biogeosciences
Discussion started: 6 December 2018

Table 2. Average biomass burning emissions (Gg) in each province from 2003 to 2017.

region/province	CO_2	CO	CH_4	NMHC	NO_x	NH_3	SO_2	BC	OC	$PM_{2.5}$	PM_{10}
Northwest	**2170.4**	**115.5**	**4.5**	**11.8**	**4.7**	**1.7**	**0.6**	**0.8**	**5.3**	**9.1**	**11.0**
Xinjiang	903.1	48.3	1.9	5.1	2.0	0.7	0.3	0.4	2.0	3.7	4.6
Gansu	292.3	15.3	0.6	1.5	0.6	0.2	0.1	0.1	0.8	1.3	1.5
Ningxia	201.5	10.4	0.4	0.9	0.4	0.1	0.1	0.1	0.6	0.9	1.0
Qinghai	93.8	4.9	0.2	0.5	0.2	0.1	0.0	0.0	0.3	0.4	0.5
Shaanxi	679.8	36.5	1.4	3.9	1.4	0.6	0.2	0.3	1.7	2.9	3.4
Northeast	**24047.9**	**1215.7**	**48.2**	**114.3**	**49.2**	**14.8**	**7.5**	**8.9**	**85.6**	**129.7**	**145.3**
Inner Mongolia	5376.6	270.9	10.8	25.0	11.0	3.3	1.7	2.0	19.5	29.2	32.5
Heilongjiang	15359.7	775.3	30.7	74.7	31.0	9.5	4.8	5.8	56.2	85.5	94.8
Jilin	1723.6	87.7	3.5	7.0	3.8	1.0	0.5	0.6	5.4	7.7	9.2
Liaoning	1588.0	81.8	3.2	7.6	3.4	1.1	0.5	0.6	4.6	7.3	8.8
North	**9633.2**	**523.7**	**19.8**	**60.0**	**20.4**	**8.5**	**2.9**	**4.1**	**21.2**	**40.3**	**48.2**
Beijing	231.1	12.6	0.5	1.5	0.5	0.2	0.1	0.1	0.5	0.9	1.1
Shanxi	1319.4	70.1	2.7	7.6	2.7	1.0	0.4	0.5	3.6	6.1	7.1
Hebei	1945.0	104.5	4.0	11.5	4.1	1.6	0.6	0.8	4.6	8.4	10.0
Shandong	2830.6	154.9	5.8	17.9	6.0	2.6	0.8	1.2	5.9	11.5	13.9
Tianjin	313.1	16.7	0.6	1.8	0.7	0.3	0.1	0.1	0.8	1.4	1.7
Henan	2993.9	165.0	6.2	19.7	6.4	2.8	0.9	1.3	5.8	11.9	14.5
Central	**15095.5**	**793.9**	**30.9**	**90.0**	**29.6**	**11.5**	**4.6**	**6.3**	**45.8**	**77.3**	**87.5**
Hubei	1773.7	95.1	3.6	10.6	3.7	1.5	0.5	0.7	4.5	7.9	9.3
Anhui	4199.2	227.5	8.6	26.3	8.7	3.6	1.3	1.8	9.9	18.4	21.6
Hunan	4994.8	259.3	10.2	28.5	9.6	3.5	1.5	2.1	16.6	26.8	29.9
Jiangxi	4127.8	211.9	8.4	24.7	7.6	2.8	1.3	1.8	14.8	24.2	26.8
Southwest	**25044.0**	**1288.4**	**52.8**	**139.1**	**45.7**	**16.1**	**7.5**	**10.0**	**86.7**	**135.0**	**153.1**
Xizang	1927.6	98.4	4.2	12.5	3.0	1.2	0.6	0.8	6.9	11.5	13.3
Sichuan	2474.9	127.8	5.0	12.7	5.1	1.7	0.8	0.9	7.8	12.4	14.1

Biogeosciences Discuss., https://doi.org/10.5194/bg-2018-468
Manuscript under review for journal Biogeosciences
Discussion started: 6 December 2018

Table 2. Continued.

region/province	CO_2	CO	CH_4	NMHC	NO_x	NH_3	SO_2	BC	OC	$PM_{2.5}$	PM_{10}
Chongqing	295.3	16.0	0.6	1.8	0.6	0.3	0.1	0.1	0.7	1.3	1.5
Yunnan	10132.4	521.2	21.2	54.8	18.7	6.4	3.1	4.0	35.7	54.7	61.3
Guizhou	2247.0	116.5	4.6	11.8	4.5	1.6	0.7	0.9	7.4	11.5	12.8
Guangxi	7966.8	408.5	17.1	45.4	13.8	4.9	2.4	3.2	28.1	43.7	50.0
Southeast	**18194.8**	**947.6**	**38.2**	**108.7**	**33.6**	**12.8**	**5.5**	**7.6**	**58.3**	**96.3**	**110.2**
Jiangsu	2982.4	164.4	6.1	19.7	6.4	2.8	0.9	1.3	5.7	11.9	14.5
Shanghai	318.7	17.5	0.7	2.1	0.7	0.3	0.1	0.1	0.6	1.3	1.6
Zhejiang	2230.0	118.5	4.5	13.5	4.5	1.8	0.7	0.9	6.2	10.8	12.4
Fujian	3791.0	192.3	7.9	23.4	6.5	2.4	1.2	1.6	14.5	23.8	26.3
Guangdong	8137.1	416.2	17.5	45.6	14.2	4.9	2.4	3.3	29.2	44.9	51.2
Macao	2.2	0.1	0.0	0.0	0.0	0.0	0.0	0.0	0.0	0.0	0.0
Hong Kong	18.2	0.9	0.0	0.1	0.0	0.0	0.0	0.0	0.1	0.1	0.1
Hainan	467.5	24.4	1.0	2.7	0.8	0.3	0.1	0.2	1.5	2.3	2.8
Taiwan	247.7	13.4	0.5	1.6	0.5	0.2	0.1	0.1	0.6	1.1	1.3

Biogeosciences Discuss., https://doi.org/10.5194/bg-2018-468
Manuscript under review for journal Biogeosciences
Discussion started: 6 December 2018

Table 3. Comparison of CO_2 emissions (Tg) from biomass burning calculated in our study with estimates made by other methods.

Year	This study	MCD64A1	GFED4s	GFASv1	FINNv1.5
2003	127.9	21.4	112.9	138.6	161.2
2004	107.0	10.7	104.5	90.3	176.4
2005	75.5	9.5	71.9	67.0	157.1
2006	93.3	11.2	91.5	76.1	185.5
2007	88.5	11.4	90.0	78.3	196.2
2008	105.1	25.1	122.4	96.3	217.1
2009	107.7	15.1	100.3	77.8	256.3
2010	92.6	12.3	80.8	76.1	213.4
2011	80.3	9.4	94.8	63.3	188.0
2012	86.7	10.9	77.5	74.0	223.3
2013	93.7	9.6	74.9	61.5	221.9
2014	120.8	20.8	114.3		157.4
2015	98.8	14.8	105.5		122.2
2016	64.5	7.4	79.3		175.7
2017	60.6	16.3			
Average	95.9	13.5	95.5	81.7	189.4

Table 4. Comparison of annual average CO_2 emissions (Tg) from each fire type calculated in our study with estimates made by other methods.

Source	This study	MCD64A1	GFED4s	FINNv1.5
forest	36.5	6.0	36.2	105.4
grassland	18.1	4.4	19.7	14.5
shrubland	9.9	0.8		31.4
cropland	31.3	2.5	38.2	38.1

5

Biogeosciences Discuss., https://doi.org/10.5194/bg-2018-468
Manuscript under review for journal Biogeosciences
Discussion started: 6 December 2018

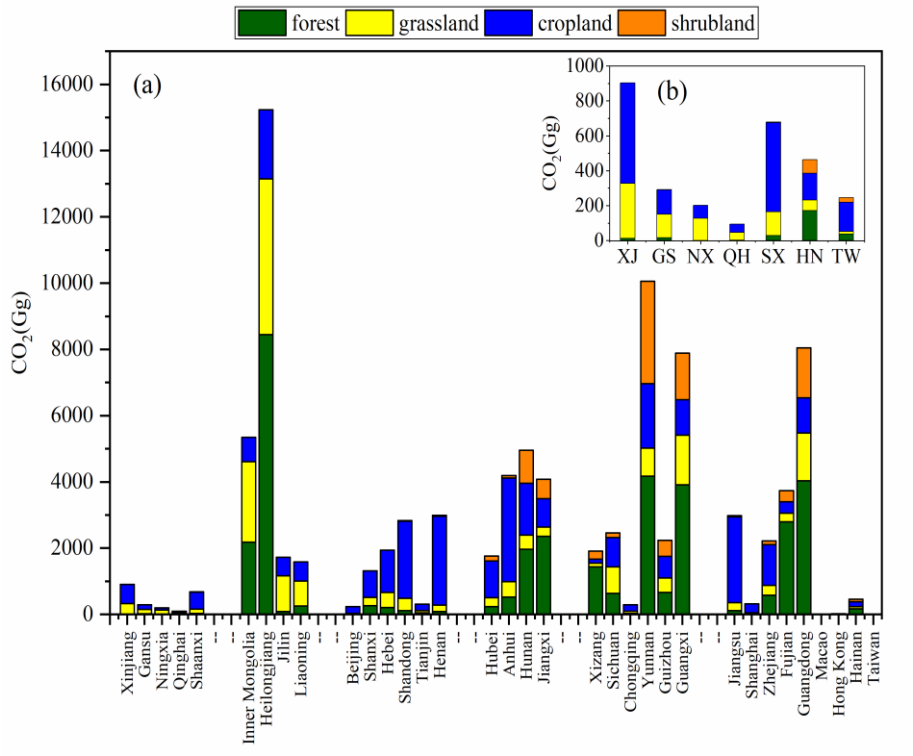

Fig.1. (a) Source-specific CO_2 emission in each province. Six provinces with relatively low emissions were shown in detail in **(b)**: Xinjiang (XJ), Gansu (GS), Ningxia (NX), Qinghai (QH), Shaanxi (SX), Hainan (HN) and Taiwan (TW). Macao and Hong Kong have minimal emissions, that is 2.2 Gg in Macao, consisting of 0.2 Gg from forest (9%), 1.5 Gg from grassland (68%), 0.1 Gg from cropland (5%), 0.4 Gg from shrubland (18%); and 18.2 Gg in Hong Kong, consisting of 8.9 Gg from forest (49%), 3.7 Gg from grassland (20%), 3.4 Gg from cropland (19%), 2.3 Gg from shrubland (12%).

Biogeosciences Discuss., https://doi.org/10.5194/bg-2018-468
Manuscript under review for journal Biogeosciences
Discussion started: 6 December 2018

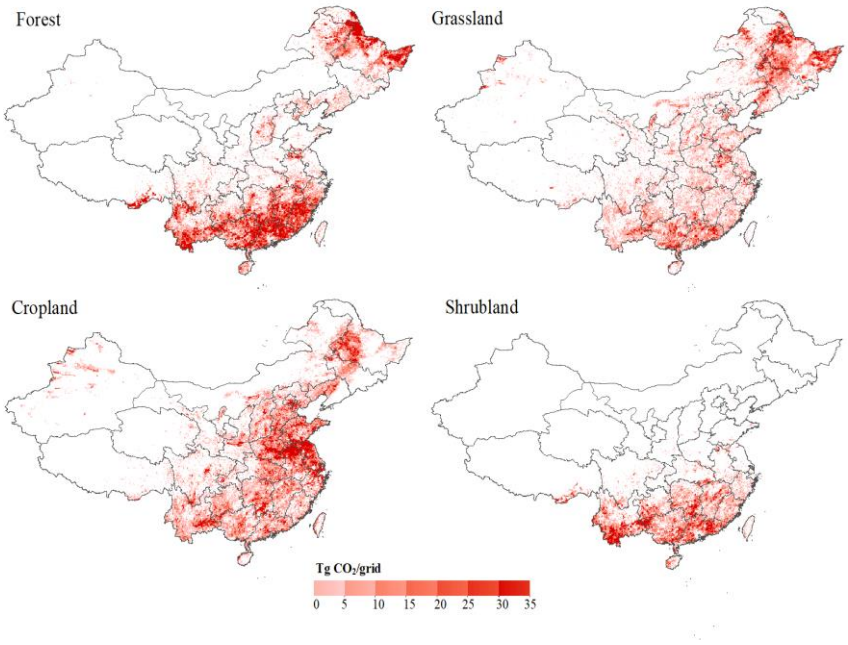

Fig.2. Spatial distribution of CO_2 emissions (Tg) from each land cover type.

Biogeosciences Discuss., https://doi.org/10.5194/bg-2018-468
Manuscript under review for journal Biogeosciences
Discussion started: 6 December 2018

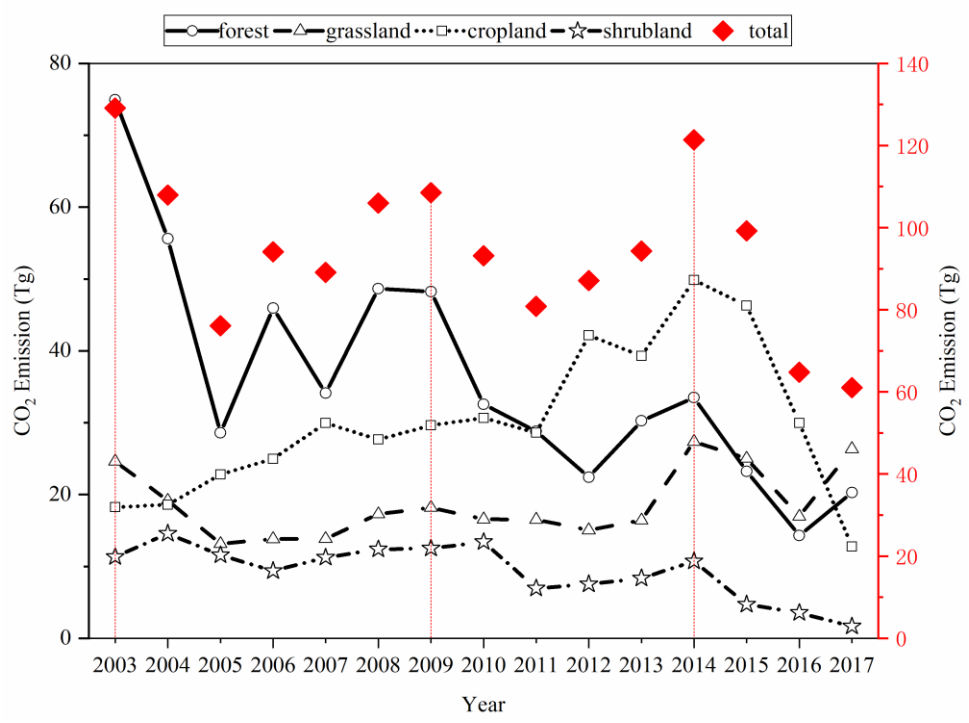

Fig.3. Annual variation in total and source-specific CO_2 emissions (Tg), 2003-2017

Biogeosciences Discuss., https://doi.org/10.5194/bg-2018-468
Manuscript under review for journal Biogeosciences
Discussion started: 6 December 2018

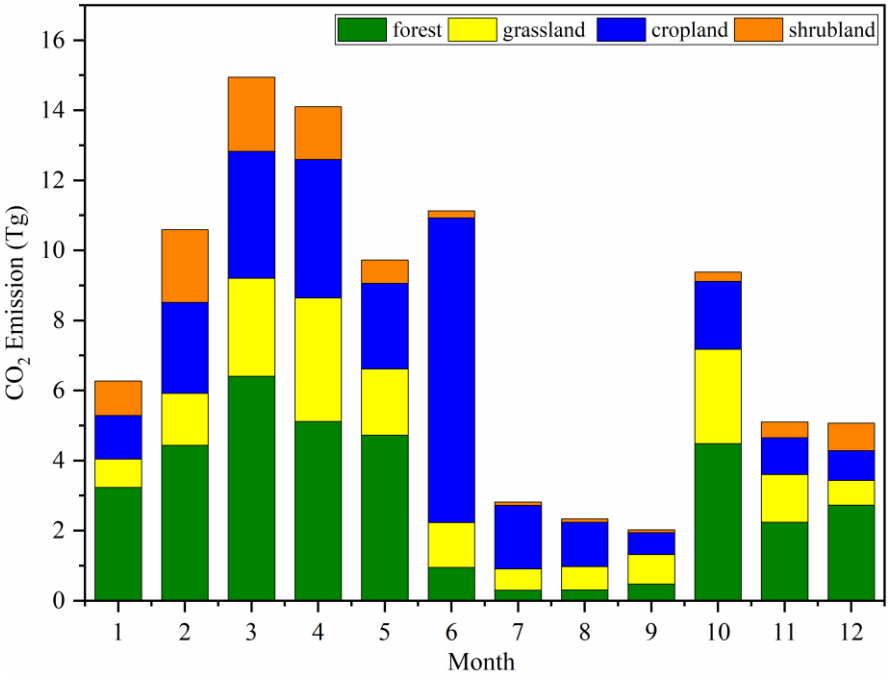

Fig.4. Monthly distributions of source-specific CO_2 emissions (Tg) in China.